

	001
	002
	003
	004
	005
	006
	007
	008
	009
	010
	011
	012
	013
	014
	015
	016
	017
	018
	019
	020
	021
	022
	023
	024
	025
	026
	027
	028
	029
	030
	031
	032
	033
	034
	035
	036
	037
	038
	039
	040
	041
	042
	043
	044
	045
	046
The Subseasonal Evolution of Indian Rainfall	
Dipole and its Local Impact in Recent Decades	
C. Sarat <sup>1*</sup> , V. Venugopal <sup>2,3</sup> and Sekhar Muddu <sup>1,4</sup>	
<sup>1</sup> *Interdisciplinary Centre for Water Research.	
<sup>2</sup> Centre for Atmospheric and Oceanic Sciences.	
<sup>3</sup> Divecha Centre for Climate Change.	
<sup>4</sup> Department of Civil Engineering,	
Indian Institute of Science, Bangalore 560012, Karnataka, India.	
*Corresponding author(s). E-mail(s): <a href="mailto:sarat@iisc.ac.in">sarat@iisc.ac.in</a> -or- <a href="mailto:csarat48@gmail.com">csarat48@gmail.com</a> ;	
Contributing authors: <a href="mailto:venu@iisc.ac.in">venu@iisc.ac.in</a> -or- <a href="mailto:venu.vuruputur@gmail.com">venu.vuruputur@gmail.com</a> ; <a href="mailto:muddu@iisc.ac.in">muddu@iisc.ac.in</a> ;	

## Abstract

Over the past two decades, the summer monsoon rainfall has shown decreasing trends over central India, with the Indo-Gangetic plains showing the most prominent changes. In particular, Bundelkhand, a subregion in the Gangetic plains, has experienced an increase in the frequency and severity of meteorological droughts. We analyse long-term rainfall data revealing two types of droughts in Bundelkhand: Type-1 droughts that coincide with the large-scale Indian monsoon droughts, and Type-2 droughts, which are localised to Bundelkhand. Our focus in this work is on the spatio-temporal evolution of rainfall during the latter category of droughts. We find that there is a distinct dipole structure in rainfall on a subseasonal scale, characterised by increased rainfall in the western India region and a decreased rainfall in east central India during July and August. Furthermore, we analyse the upper- and lower-level atmospheric circulation changes responsible for the subsidence during Type-2 droughts. The rainfall deficit during July and August appear to be associated with a midlatitude stationary Rossby wave which induces an anomalous anticyclone over western North Pacific which drives easterlies over the south China Sea into east central India, that in turn reduce the regional moisture influx. At the same time, the Rossby wave also induces an anomalous cyclonic circulation over northwest India and Pakistan,

047 increasing moisture convergence from the Arabian Sea, leading to enhanced con-  
048 vection over west India. During September, the high-pressure region over Tibetan  
049 Plateau migrates further southward into central India, increasing (decreasing)  
050 subsidence (convection). Taken together, a combined effect of intraseasonal vari-  
051 ations in the midlatitude jet and the circulation over western North Pacific and  
052 Tibetan Plateau are responsible for the observed rainfall dipole pattern. At the  
053 downstream end, we find that the enhanced soil stress (dryness) owing to reduced  
054 rain may have a role to play in the much-reported depletion of groundwater  
055 storage in northwest India in general.  
056

057 **Keywords:** Indian Monsoon, Drought, Rainfall Dipole, Regional climate  
058  
059  
060

## 061 1 Introduction

062

063 The Indian monsoon is an annual climate phenomenon that in rainfall from June  
064 to September (JJAS) over India, with the summer season rainfall accounting for 70-  
065 90% of the total annual rainfall over India. It is modulated by interactions between  
066 land, atmosphere and the tropical Indian Ocean at a range of space and time scales  
067 (Webster et al., 1998). Understanding the spatio-temporal variability of Indian sum-  
068 mer monsoon rainfall (ISMR) is essential for forecasting and policy making, as India's  
069 agricultural yield in the Kharif season depends on summer season rainfall (Gadgil and  
070 Gadgil, 2006). Indian monsoon responds to external drivers such as sea surface tem-  
071 perature (SST) patterns, climate change, and low-frequency climate variability. The  
072 monsoon's internal variability is often seen to be responsible for the active and break  
073 spells in rainfall which, in turn, can be modulated by external drivers. There has been  
074 substantial work done over the past several decades to understand the subseasonal  
075 and seasonal variability of monsoon rainfall and its seasonal extremes (i.e., droughts  
076 and floods). In particular, efforts have focussed on identifying slow-varying oceanic  
077 markers that have a stranglehold on monsoon variability, such as the phases of El  
078 Niño Southern Oscillation (ENSO), namely, El Niño and La Niña respectively (Moo-  
079 ley and Parthasarathy, 1983; Goswami, 1998). Furthermore, the positive (negative)  
080  
081  
082  
083  
084  
085  
086  
087  
088  
089  
090  
091  
092

phase of the Indian Ocean Dipole (IOD) has been associated with excess (deficit) in seasonal rainfall of ISM. (Ashok et al., 2001; Gadgil et al., 2004). More recently, there is evidence for extratropical influences from the Atlantic Ocean modulating interannual and subseasonal variability of the Indian monsoon. (Rajeevan and Sridhar, 2008; Yadav, 2009; Boers et al., 2019; Borah et al., 2020).	093 094 095 096 097 098 099 100 101 102 103 104 105 106 107 108 109 110 111 112 113 114 115 116 117 118 119 120 121 122 123 124 125 126 127 128 129 130 131 132 133 134 135 136 137 138
On the secular changes front, several studies have documented a decreasing trend in ISMR over central India in the global warming era. While central India and the Indo-Gangetic Plains have experienced an accelerated decrease in the seasonal quantum of rainfall over the past two decades, western India has shown an increase in ISMR, effectively resulting in an apparent dipole pattern in rainfall (Mishra et al., 2012; Jiang and Ting, 2017; Athira et al., 2023). Besides the changes in rainfall manifesting as a dipole, the frequency and severity of extreme daily rainfall events in central and western India have increased significantly during the past century (Goswami et al., 2006; Roxy et al., 2017). Some studies have attributed the ISMR dipole pattern to long-term increase in sea surface temperature (SST) in the western and Equatorial Indian Ocean (Mishra et al., 2012; Roxy et al., 2015; Goswami, 2023). In addition, the negative phases of IOD favour moisture convergence (divergence) over western India (central India), resulting in the ISMR dipole (Behera and Ratnam, 2018). Furthermore, the ISMR dipole pattern seems to be prominent during a La Niña year, preceded by a La Niña in the previous winter, while transitions from winter El Niño to summer La Niña do not appear to be favourable for the occurrence of a dipole in rainfall patterns. These “Rogue La Niñas” may have a role to play in decreased rainfall over central India even when the Pacific is cooler, thereby altering the canonical relationship between ISMR and Pacific (Gadgil et al., 2023; Sharma et al., 2024).	
There is also some evidence that a westward expansion of the west Pacific subtropical high (WPSH) and increased active tropical cyclone activity over the western north Pacific are responsible for decreased ISMR over central India (Darshana et al.,	

139 2020; Chaluvadi et al., 2024). The Tibetan Plateau, located northeast of India, influ-  
140 ences ISMR on an interannual time scale to the extent that monsoon rainfall and the  
141 Tibetan Plateau can be considered a coupled system. At a seasonal level, the heating  
142 over Tibetan Plateau significantly correlates with early and late season rainfall during  
143 June and September when the Somali Jet is relatively weaker compared to the peak  
144 monsoon period of July and August (Rajagopalan and Molnar, 2013). However, there  
145 is some evidence that differential heating patterns over Tibetan Plateau modulate the  
146 low-level monsoon jet (westerlies), thereby influencing regional vapour transport. The  
147 latent heating over Tibetan Plateau strengthens the westerlies, increasing rainfall over  
148 northwest India. At the same time, the vapour transport from the Bay of Bengal into  
149 central India decreases, resulting in the rainfall dipole (Jiang and Ting, 2017). Finally,  
150 the surface pressure patterns over Tibetan Plateau also could be responsible for the  
151 occurrence of ISMR dipole. Increasing surface pressure over Tibetan Plateau inten-  
152 sifies lower-level easterlies in northwestern India while decreasing mid-tropospheric  
153 northwesterlies in East India and the Indo-Gangetic Plains (Singh et al., 2022).  
154

155 Most studies have attempted to link the formation of rainfall dipole to long-term  
156 and seasonal changes in SST patterns and seasonal shifts in the tropospheric circula-  
157 tion over western North Pacific. However, very few studies explored the subseasonal  
158 evolution of the rainfall dipole, although they focused on specific years when the  
159 dipole pattern was evident. To that end, in this study, we perform a composite analy-  
160 sis across years to gain insights into the interannual and subseasonal evolution of the  
161 ISMR dipole, as well as perform a diagnostic analysis of the upper level atmospheric  
162 circulation to identify potential local and remote drivers of observed subseasonal vari-  
163 ability leading to the dipole in rainfall patterns. Specifically, as our analysis revealed,  
164 our focus in part is on a smaller region within the Indo-Gangetic Plains, namely, Bun-  
165 delkhand, which appears to have been the most affected region over the past two to  
166 167  
168

three decades. This region also falls in the belt where significant depletion of groundwater has been reported. Thus, our study while investigating the large-scale factors influencing the dipole pattern in rainfall and its subseasonal evolution, also presents an analysis of impact at the downstream end (namely, soil moisture and groundwater) over the Bundelkhand region.

The outline of our work is as follows: Section 2 presents the data - observations and reanalysis - used in our study, along with the methodology. Section 3 presents the main results of our investigation, with much of it focussing on the rainfall patterns during drought years and the plausible pathways that may have led to the subseasonal variability; the last third of this section (Section 3.4) presents how this rainfall variability may have had a bearing on the local hydrology, specifically on changes in soil moisture and groundwater. We conclude by presenting a summary of our main findings, along with a discussion of a few open-ended questions in Section 4.

## 2 Data and Methods

## 2.1 Data

We use a suite of datasets - both observational and reanalysis - for our study: observed rainfall, soil moisture and groundwater, along with dynamical variables from reanalysis describing the state of the upper atmosphere for the diagnostic part of our analysis. The focus is on June to September monsoon months, referred to henceforth as JJAS.

For rainfall, the daily gridded rainfall at 1° resolution for 1901-2023 from the Indian Meteorological Department (IMD) ([Rajeevan et al., 2006](#)), along with the All India area-weighted mean Summer Monsoon Rainfall (AISMR), developed by the Indian Institute of Tropical Meteorology (IITM; available at <https://www.tropmet.res.in>), are used. The latter dataset is based on a homogeneous rainfall record from 306 rain gauges across India. We use this dataset primarily to identify all-India droughts, as it

231 is considered to be a reliable index of AISMR variability. (Parthasarathy and Mooley,  
232 1978; Parthasarathy et al., 1994),

234 On the diagnostic analysis front, we use the fifth generation atmospheric reanalysis  
235 of the global climate from the European Centre for Medium-Range Weather Forecasts  
236 (ECMWF; <https://cds.climate.copernicus.eu>) (ERA5; Soci et al. (2024)). The daily  
237 reanalysis fields for zonal wind ( $u$ ), meridional wind ( $v$ ), vertical pressure velocity ( $\omega$ ),  
238 Geopotential Height (GPH), vorticity and vertically integrated moisture divergence  
239 (VIMD) are obtained at a spatial resolution of  $0.25^\circ$ .  
240

241 For analysing the impact of changes in rainfall at the downstream end, namely,  
242 the response of the land surface, the daily profile of soil moisture (in  $kg/m^2$ ) for  
243 2003-2023 was obtained from the Global Land Data Assimilation System (GLDAS)  
244 Catchment Land Surface Model (CLSM) (Li et al., 2020) at a resolution of  $0.25^\circ$ .  
245 The depth to groundwater level (DGWL) data for wells in the Bundelkhand region  
246 was accessed from the Central Groundwater Board (CGWB) on the India - Water  
247 Resources Information System (<https://indiawris.gov.in/wris/>) portal.  
248

249

250

251

252

253

254

255

256

257

258

259

260

## 261 2.2 Methodology

262

263 Most of our analysis is based on the anomalies of various observables and reanalysis  
264 fields. Specifically, to understand the subseasonal evolution of a given field  $A$ , we define  
265 daily anomalies, for a given day ( $day$ ) in a year ( $yr$ ), at a location  $(x, y)$  during the  
266 summer monsoon months of June through September. These anomalies, denoted by  
267  $A' (x, y, day, yr)$ , are estimated in a conventional way as the deviation from its daily  
268 climatology:

269

270

271

272

273

274

275

276

$$A' (x, y, day, yr) = A (x, y, day, yr) - \frac{1}{N_{yr}} \left( \sum_{yr=1}^{N_{yr}} A (x, y, day, yr) \right) \quad (1)$$

From these daily anomalies, we construct  $j$ -day anomalies,  $A'_j(x, y, yr)$  as a sum of  
daily anomalies over  $j$  days. 277  
278  
279  
280

$$A'_j(x, y, yr) = \sum_{day=1}^j A(x, y, day, yr) \quad (2) \quad 281  
282  
283  
284$$

where  $N_{yr}$  is the available number of years of observations or reanalysis data. The field  
 $A$  in our analysis includes rainfall, wind, geopotential height (GPH) and vorticity. 285  
286  
287  
288

Specific to the Indian monsoon context, a drought year is defined by the India  
Meteorological Department, based on the percentage deviation of JJAS rainfall ( $D_i$ )  
from the long-term mean (Eq. 3) or, equivalently, a normalised rainfall deviation ( $Z_i$ ).  
This translates to  $D_i \lesssim -10\%$  ( $Z_i \leq -1$ ) for all-India (Mooley and Parthasarathy,  
1983; Rasmusson and Carpenter, 1983), and  $D_i \leq -17.3\%$  ( $Z_i \leq -1$ ) for Bundelkhand  
(see Table 1). 289  
290  
291  
292  
293  
294  
295  
296  
297  
298  
299

$$D_i = \left( \frac{P_i - \bar{P}}{\bar{P}} \right) \times 100\% \quad (3) \quad 300  
301$$

$$Z_i = \left( \frac{P_i - \bar{P}}{\sigma} \right) \quad 302  
303  
304$$

where  $P_i$  is the total seasonal (JJAS) rainfall for a given year  $i$  and  $\bar{P}$ ,  $\sigma$  are its  
long-term mean and interannual standard deviation, respectively. 305  
306  
307  
308  
309  
310  
311  
312

### 3 Results

As alluded to in the Introduction, our discussion centres around Bundelkhand region  
in the Indo-Gangetic Plains, where the changes in rainfall appear most prominent.  
This focus is in part motivated by earlier studies that have highlighted a dipole of  
changes in rainfall between central Gangetic plains and west India region (Mishra  
et al., 2012; Athira et al., 2023). A preliminary empirical orthogonal functional (EOF)  
analysis of ISMR clearly illustrates this dipole (Fig. 1). It is worth noting that the  
313  
314  
315  
316  
317  
318  
319  
320  
321  
322

323 dipole shows up as the most dominant mode of interannual variability (unlike previous  
324 studies which report this as the 2nd EOF mode). The reason for this is the kind of  
325 normalisation we used. While other studies have normalised rainfall anomalies with  
326 interannual standard deviation, we use the climatology of seasonal standard deviation  
327 for our normalisation, before performing an EOF decomposition (see “Supplementary  
328 Information” for details of normalisation). The rationale for such a choice is that there  
329 is substantial spatial variability in rainfall and to make it homogeneous and more  
330 amenable to an EOF type of analysis, the local seasonal standard deviation is more  
331 apt. In and of itself, this kind of normalisation does not alter the larger, essential  
332 message, i.e., that there is a dipole in rainfall changes: it only serves to amplify the  
333 strength of the dipole.  
334

341 A stand-out feature from this preliminary analysis is an apparent regime shift in  
342 the principal component of the first EOF mode (PC-1) shown in Fig. 1b. Prior to  
343 the turn of this century, PC-1 is predominantly negative. However, post-2000, the  
344 PC-1 time series transitions to a positive phase with a marked increase in amplitude  
345 and variance. This shift strongly suggests that the dipole pattern of rainfall (taken in  
346 conjunction with the opposite signs of EOF loading in Fig. 1a), has become a more  
347 frequent and intense mode of interannual variability in recent decades. This finding  
348 provides further justification to focus on these localised droughts which have become  
349 more prevalent in the recent two decades.  
350

356 From Figs. 1a, b, the region where the reduction in summer monsoon rainfall is  
357 most evident is Bundelkhand, which lies towards northern central India, bordering  
358 the states of Madhya Pradesh and Uttar Pradesh (Fig. S1). Bundelkhand comprises  
359 13 districts in the Indo-Gangetic Plains, contributing to a total area of approximately  
360 73,700 km<sup>2</sup> (top right panel of Fig. S1). The land use in this region is predominantly  
361 agricultural and highly reliant on rainfall. The average annual rainfall in this region is  
362 approximately 960 mm, with JJAS rainfall contributing nearly 90%. Bundelkhand is  
363

infamous for its severe water scarcity due to frequent droughts and ineffective water management strategies. The water scarcity in this region has resulted in poor socioeconomic conditions and lowered agricultural yields (Sharma, 2023; Patidar et al., 2024). To better understand the zonal asymmetry in rainfall, manifesting as a dipole, we focus on this region ( $22\text{-}27^{\circ}\text{N}$ ,  $78\text{-}83^{\circ}\text{E}$ ; dashed rectangle in Fig. 1a) for in-depth analysis.

### 3.1 Drought Categories

To identify droughts, we compare the interannual anomalies of the all-India summer monsoon rainfall (see Section 2.1) with those of rainfall over Bundelkhand, our region of interest (Fig. 2). Between 1901 and 2023, India experienced 24 droughts (Fig. 2a; years when the departure from mean is less than -10%). During this same period Bundelkhand experienced 20 droughts (Fig. 2b). The clustering of droughts in Bundelkhand over the past two decades is evident, with the region experiencing severe rainfall deficit, on an average, once every two years from 2002 to 2020. In both panels of Fig. 2, the “blue” bars represent those years when *only Bundelkhand* experienced severe deficit, while the “red” bars represent Bundelkhand droughts that coincide with large-scale Indian monsoon droughts. In order to understand the features of these “isolated” and localised droughts in Bundelkhand, we consider the following two categories:

- Type-1 Drought: A drought year over India coincides with one in Bundelkhand.
- Type-2 Drought: A drought year exclusive to Bundelkhand.

Bundelkhand experienced 12 Type-1 (“red” bars in Fig. 2) and 8 Type-2 (“blue” bars in Fig. 2) droughts during 1901-2023 (see also Table 2). Type-1 droughts are in fact a subset of the large-scale ISMR droughts that have been studied extensively, with a majority of these years linked to El Niño (Krishnamurthy and Goswami, 2000; Timmermann et al., 2018; Kiran Kumar and Singh, 2021; Ratna et al., 2024). Our focus in this work is on Type-2 drought events, which are localised to Bundelkhand.

415 Curiously enough, Type-2 droughts appear to coincide with weak to moderate La Niña  
416 like conditions in equatorial Pacific (Fig. S2).  
417

418  
419  
420

### 421 **3.2 Dipole Pattern of Rainfall**

422  
423

#### *424 Seasonal Footprint*

425 Fig. 3 shows the spatial distribution of seasonal (JJAS) rainfall climatology and com-  
426 posites of the corresponding anomalies for both drought types, respectively, during  
427 the period 1901-2023. As expected, Type-1 droughts (Fig. 3b) are characterized by  
428 large-scale rainfall deficits that engulf a significant portion of the country. Specifically,  
429 Type-1 droughts result in an average seasonal rainfall deficit of more than 150 mm,  
430 primarily concentrated over central India and the Indian western coast. Furthermore,  
431 other parts of the country (e.g., peninsular India), experience an average seasonal rain-  
432 fall deficit of approximately 100 mm, whereas northeast India experiences normal to  
433 above-normal rainfall. This northeast / rest of India contrast in excess/deficit rainfall  
434 is a well-known feature during El Niño droughts, particularly during the past century  
435 (Saikranthi et al., 2018; Kiran Kumar and Singh, 2021). In contrast, Type-2 droughts  
436 (Fig. 3c) are characterized by rainfall deficit that is confined primarily to Bundelk-  
437 hand and a few parts of northeast India. During a Type-2 drought, while central  
438 India receives near-normal rainfall, the western and southern parts of India experience  
439 above-normal rainfall (broadly consistent with the EOF analysis presented in Fig. 1).  
440 This dipole pattern of decreased JJAS rainfall over Bundelkhand and concurrently  
441 increased rainfall over western and southern India is the primary distinguishing factor  
442 between Type-1 and Type-2 droughts.

443 An additional way to characterise this distinction between the two categories of  
444 droughts is the accumulation of rainfall deficit in Bundelkhand, along with the west  
445 India sector (WI: 17-25°N, 69-78°E; see larger dashed rectangles in Figs. 3a, c). The  
446 average build up of rainfall deficit in these two regions (solid curves) along with their

intra-drought spread (shading) are shown in Fig. 4. It is quite clear, and not surprising, 461  
that when the droughts are large-scale in nature (Type-1) rainfall deficit is seen nearly 462  
everywhere (declining solid red and black curves in the left panel of Fig. 4). Contrast 463  
this with the case of localised droughts, shown in the right panel of Fig. 4, one can 464  
readily see the temporal behaviour of the aforementioned dipole structure: a gradual 465  
buildup of rainfall deficit in Bundelkhand (solid blue curve), while the west India region 466  
(solid black curve) shows above normal rainfall with a particularly rapid increase over 467  
a period of 45 days, spanning from mid-July to end-August. 468

The intra-category heterogeneity seen in Fig. 4b is also evident in the spatial 469  
distribution of rainfall anomalies for each of the Type-2 drought years (Fig. S3). 470  
These spatial patterns point to the possibility that the east-west rainfall dipole may 471  
be a recent phenomenon, i.e., more apparent in the Type-2 droughts of the past two 472  
decades compared to those that occurred during the early 20th century. **Indeed, this** 473  
**observation is consistent with the post-2000 regime shift identified in the principal** 474  
**component of EOF Mode 1 (Fig. 1b).** In fact, a comparison of the contrast between 475  
the spatial patterns of rainfall during pre- and post-2000 Type-2 droughts (Fig. 476  
S3a-c *vs.* Fig. S3d-h) also appears to highlight this transition, although the sample 477  
size for either pre- and post-2000 droughts is arguably not large. This suggests that 478  
perhaps the dipole structure may have become prominent only in recent decades. For 479  
example, the rainfall deficit region was mostly confined to Bundelkhand during 2006 480  
and 2007. In these two years, Bundelkhand experienced an average rainfall deficit of 481  
greater than 250 mm, while the surrounding region experienced excess rainfall of a 482  
similar magnitude. In 2010, the dipole shows a marginal shift to the east, resulting 483  
in Bundelkhand, east and northeast India experiencing a rainfall deficit. Also, in the 484  
same year, the southwestern coast of India, where the climatological rainfall is nearly 485  
2000 mm, experienced a deficit of over 250 mm. Even though the rainfall dipole pat- 486  
tern was slightly subdued in 2017 and 2020, Bundelkhand remains the centrepiece for 487  
488  
489  
490  
491  
492  
493  
494  
495  
496  
497  
498  
499  
500  
501  
502  
503  
504  
505  
506

507 rainfall deficit, further solidifying the need to understand this peculiar localisation.

508

509

510 *Subseasonal Variability of the Dipole Pattern*

511

512 The discussion, thus far, has centred around seasonal rainfall and its deficit. Given  
513 that much of the monsoon rainfall - be it a burst of rainfall or a period of quiescence -  
514 manifests on shorter timescales, often referred to as “active” and “break” spells (Pai  
515 et al., 2016; Saha et al., 2023), we investigate the subseasonal evolution of rainfall and  
516 its spatial distribution, with particular emphasis on Bundelkhand and its neighbouring  
517 regions. For compactness sake, here, we choose to highlight and discuss the 20-day  
518 accumulation of rainfall anomalies for the two types of droughts (Fig. 5 and Fig.  
519 523). During early June, rainfall is near-normal over most of India (Fig. 5a; see also  
520 the cumulative curves hovering mostly around zero in Fig. 4b). Subsequently, the  
521 first indications of a rainfall dipole emerge between late June and early July, when  
522 Bundelkhand and parts of northeast India experience decreased rainfall (Fig. 5b). This  
523 is, once again, consistent with the separation between an increasing and a decreasing  
524 cumulative rainfall anomalies curve for western India and Bundelkhand, respectively  
525 (black and blue curves between day 20 and 40 in Fig. 4b).

526       During this period, we observe a similar pattern of decreased rainfall over the  
527 western Indian coast for Type-1 (Fig. S4b,c) droughts as well. However, the negative  
528 rainfall anomaly in Type-1 droughts during this period covers a significant part of  
529 central India, unlike Type-2 droughts (compare Fig. S4b with Fig. 5b). During the sec-  
530 ond half of July, the peak monsoon season, the dipole structure of rainfall in Type-2  
531 droughts becomes increasingly evident as we observe a band of decreased rainfall diag-  
532 onally across east-central and northwest India (Fig. 5c). Although a similar pattern of  
533 rainfall deficit appears over central India in Type-1 droughts at this stage (Fig. 5c),  
534 the peninsular Indian regions show contrasting behaviour (increase in Type-2 with  
535 normal to less than normal in Type-1). As the season progresses, the dipole shifts  
536

to the east during early August, and the region of decreased rainfall aligns broadly with the monsoon trough's climatological position (Fig. 5d). This eastward shift in the dipole is characterised by decreased rainfall over east-central and northern India and increased rainfall over western and peninsular India. At this stage, western India exhibits increased rainfall with a daily anomaly  $\geq 4$  mm/day. In comparison, Bundelkhand and northeastern India experience decreased rainfall with a daily anomaly of  $\leq -5$  mm/day. Between late August and early September (Fig. 5e), even though the magnitude of rainfall deficit (excess) becomes subdued over Bundelkhand and northeast India (western India), the broader dipole structure is still evident. As the monsoon retreats in the second half of September, the zonal rainfall asymmetry dampens, with east-central India and western India now receiving reduced rainfall (Fig. 5f).

To summarise, Type-2 drought conditions reveal similar trends in rainfall between Bundelkhand and western India until early-to-mid July, followed by a divergence of cumulative curves as the latter region experiences more than normal rainfall, while Bundelkhand rainfall trajectory continues its downward trend, leading to a seasonal shortfall approximating 220 mm. Thus, our characterisation of the drought as having a “subseasonal” nature refers specifically to the evolution of this dipole pattern. While rainfall deficit over Bundelkhand persists through the season, the distinct dipole structure with concurrent excess rainfall over western India is most pronounced during a 6 to 8-week period from mid-July to early September (Fig. 4b). It is this intensification and subsequent waning of the dipole within the JJAS season that constitutes its subseasonal evolution. This timeframe is also consistent with the dominant timescales of monsoon's intraseasonal oscillations, suggesting a potential link between the dipole's evolution and broader subseasonal variability. (It is worth noting that we also analysed the spatial distribution of 10-day accumulation of rainfall anomalies (not shown); apart from the fact that one would expect an increase in variability at smaller timescales, it does not alter the essence of our main finding.).

599 **3.3 Atmospheric Circulation**

600

601 In order to understand how the upper atmosphere circulation features we perform a  
602 diagnostic analysis of the ERA5 reanalysis data. Again, given that Type-1 droughts  
603 are more large-scale, and likely driven by El Niño and extensively studied, our focus  
604 here is more on the rainfall deficit localised over Bundelkhand region. It is increas-  
605 ingly being recognised that extreme weather events (seasonal or short duration) across  
606 the Asian summer monsoon domain, such as droughts, floods, and heat waves, are  
607 significantly modulated by the interplay between external forcing (e.g., anomalous  
608 SSTs) and internal atmospheric variability (Deng et al., 2019). This internal vari-  
609 ability includes dynamics like teleconnections linking concurrent extremes in different  
610 regions (Fu et al., 2024) and extratropical Rossby waves influencing summer monsoon  
611 rainfall on intraseasonal timescales. (Borah et al., 2020; Fu et al., 2024).

612

613 Here, we focus on late July to early September, the period when the dipole structure  
614 in Type-2 droughts is most prominent; specifically, July 20-31, August 1-15 and August  
615 24 - September 8. For these selected time periods, we find that ERA5 captures the  
616 observed rainfall features quite accurately in terms of the vertically integrated moisture  
617 fluxes (not shown).

618

619 We begin with an analysis of geopotential height (GPH), wind and vorticity anom-  
620 alies at select pressure levels, on subseasonal scales during JJAS. The wind anomalies  
621 are shown at all chosen pressure levels; GPH anomalies are shown for 200 and 500 hPa,  
622 and vorticity anomalies shown at the lower levels (700 and 850 hPa). Fig. 6 shows  
623 composites of anomalies of GPH (shading), vorticity (shading) along with wind vec-  
624 tors for the first two time periods (mid July to mid-August) and Fig. 7 shows the  
625 same quantities for the late-August/early-September period. In late July, the circum-  
626 global Rossby wavetrain modulates increased and decreased GPH regions in the upper  
627 troposphere (Fig. 6a; 200 hPa). This results in a region of increased GPH over north-  
628 ern Tibetan Plateau (TP) at the 200 hPa level. However, in the mid-troposphere  
629

630

(Fig. 6b; 500 hPa), the increased GPH over TP expands southwards into a significant portion of east-central India. At this level, we also observe a band of anomalous easterlies stretching from the western North Pacific to eastern India. The western North Pacific anticyclone favours the formation of these easterlies, which flow from the South China Sea zonally into central India, resulting in a mid-tropospheric anticyclone over the region. The vorticity forcing from this mid-tropospheric anticyclone drives a barotropic response, resulting in an anticyclonic cell in the lower troposphere (700, 850 hPa; Figs. 6c, d) over central India. The anomalously strong easterlies at 700 hPa oppose the monsoon southwesterlies flowing into east-central India. Simultaneously, the interaction between these easterlies and the climatological monsoon flow establishes an anomalous cyclonic circulation over northwest India and adjoining regions. This downstream development, where the upper-level wave train appears to force a lower-level cyclonic response, is a key feature distinguishing the dynamics of Type-2 drought events. This circulation enhances the southwesterly flow from the Arabian Sea into western India, promoting moisture convergence and convection there. This results in break-like conditions and rainfall deficit over east-central India, while western India experiences enhanced rainfall, consistent with the vorticity patterns in Fig. 6d. This proposed regional dipole mechanism is notably different from the circulation during Type-1 droughts, which are known to be characterized by a large-scale anomalous anticyclone and widespread subsidence across most of India, consistent with a canonical El Niño response (Fig. S5).

During the first half of August, in Type-2 drought events, the midlatitude Rossby wavetrain at 200 hPa curves southward down to 30°N (Fig. 6e). During this period, the strengthening of the anomalous anticyclone over the Tibetan Plateau (TP) is also evident. This anomalous anticyclonic cell over TP disrupts the flow of monsoon southwesterlies into the Himalayan foothills and east-central India, where the climatological monsoon trough is located at this time of the season. The monsoon jet strengthens

in the mid-troposphere, and the easterlies flowing into central India weaken. However, this strengthened monsoon flow creates significant zonal shear as it interacts with the anomalous easterly flow on the southern flank of the Tibetan High (Fig. 6e,f). This interaction establishes a distinct vorticity dipole in the lower troposphere (Fig. 6g,h), with cyclonic shear enhancing moisture convergence over western India and anticyclonic shear promoting subsidence over east-central India. This circulation-driven vorticity pattern is therefore directly responsible for the pronounced rainfall dipole observed during this period. In contrast, the circulation for Type-1 droughts during August does not show a southward migration of the Rossby wavetrain in the upper troposphere (Fig. S5 e,f). However, during this period, the strengthened southwesterlies in the lower troposphere result in an anomalous band of cyclonic vorticity across India signaling an active phase of the monsoon within the broader drought season (Fig. S5 g,h).

Between late August and early September (Fig. 7), during Type-2 drought events, the upper tropospheric anomalous anticyclone over the Tibetan Plateau gets relatively weaker. Additionally, the anomalous western North Pacific anticyclone at 200 hPa also weakens and expands eastward during this period. However, at the 500 hPa level, the anticyclonic cell and the region of increased geopotential height migrate southward over east-central India, strengthening the anomalous easterlies over the region. In the lower troposphere, this results in a distinct zonal shear which strengthens the anticyclonic vorticity over east-central India inducing moisture divergence. Concurrently, the persistent anomalous cyclonic circulation over northwest India maintains cyclonic vorticity and strengthens moisture-bearing winds from the Arabian Sea. This east-west dipole in vorticity directly drives the zonal rainfall asymmetry contributing to the observed rainfall dipole pattern until mid-September. This subseasonal migration and evolution of regional circulation cells in Type-2 events differs from the persistent,

large-scale subsidence that characterizes Type-1 droughts from late August to early September (see Fig. S6). 737  
738  
739

To further understand the vertical structure of the atmosphere during Type-2 droughts, we analyse changes in the local Walker (averaged over the Indian latitudinal zone of 17-27°N) and Hadley (averaged over the Indian longitudinal zone of 69-83°E) circulations for those periods when the rainfall dipole is most prominent (Fig. 8). 740  
741  
742  
743  
744  
745  
746  
747  
748  
749  
750  
751  
752  
753  
754  
755  
756  
757  
758  
759  
760  
761  
762  
763  
764  
765  
766  
767  
768  
769  
770  
771  
772  
773  
774  
775  
776  
777  
778  
779  
780  
781  
782

This vertical circulation is evidently different from the large-scale, widespread subsidence observed across the entire Indian subcontinent during Type-1 droughts (see Fig. S7 for comparison). This circulation is also concurrent with a zone of anomalous subsidence over the equator that extends further to 10°S. When the zonal asymmetry in rainfall dipole starts weakening in early September, we observe an anomalous shallow descending motion to the west of 75°E, indicating decreased convection over western India. During this period, the deep subsidence in the 75-100°E longitude band indicates decreased convection over east-central India. Around the same time, the local Walker circulation appears to shift southward, evident in the strong ascent from the equator to 10°N (Fig. 8c, d), indicating increased convection to the south of India. As a result, peninsular India now experiences near-normal rainfall in early September instead of increased rainfall (as was the case during August). However, during this early September period, the 20-30°N latitude band still experiences anomalous descending motion, consistent with

783 decreased rainfall over north India (including Bundelkhand). Overall, this sub-seasonal  
784 evolution aligns well with the seasonally averaged (JJAS) vertical velocity anomaly  
785 patterns observed during Type-2 droughts (Fig. S8b, d). The composites clearly show  
786 the characteristic mid-tropospheric dipole over India, with strong anomalous subsi-  
787 dence over east-central India and ascent over western and peninsular India (Fig. S8  
788 b). Furthermore, weak anomalous ascent is seen over the Maritime Continent and  
789 Western Pacific, indicating a distinct large-scale circulation pattern.  
790

791

792

793

794

795

796

### 797 **3.4 Effects on local hydrology**

798

799 Thus far, we have investigated the upper atmospheric circulation features, and plau-  
800 sible pathways leading to localised droughts in the Bundelkhand region, which appear  
801 distinctly different from conventional large-scale Indian droughts in terms of the  
802 space-time structure of evolution of rain. Equally, if not more, importantly, such meteo-  
803 rological droughts can potentially have a significant impact on the region's agricultural  
804 output, threatening food security and overall socio-economic stability. In particular,  
805 the response of soil moisture to rainfall is highly non-linear, and the propagation of a  
806 meteorological drought into what one might deem a "soil moisture drought" depends  
807 on antecedent soil moisture conditions ([Zhu et al., 2021](#)). Understanding the soil mois-  
808 ture variability during June–October is therefore essential, as it is the Kharif crop  
809 season for agriculture in India. To this end, we quantify the footprint of these two  
810 categories of droughts on soil moisture, which typically exhibits a temporally lagged  
811 response to meteorological droughts due to the inherent buffering capacity of soils.  
812

813

814 Fig. 9 shows the composites of normalised monthly soil moisture anomalies during  
815 Type-1 (top row) and Type-2 (bottom row) droughts for the period July to October,  
816 to account for the lagged response of the land surface to rain, at least as seen in  
817 soil moisture. The distinction between the two types of droughts on the downstream  
818 end, namely, in terms of soil moisture patterns, is even more striking than in the  
819

820

rain patterns discussed earlier. In particular, during Type-1 droughts, we reported  
that most of central India receives significantly less than normal rain during JJAS;  
correspondingly, the soil moisture deficit is spread across a large part of the Indo-  
Gangetic Plains (Figs. 9a-d). Additionally, we also observe increased soil stress (i.e.,  
decreased soil moisture) in the west India region, and peninsular and southern India  
regions, as they too receive less-than-normal rainfall (see Fig. 3b or Fig. S4). The soil  
stress persists well into the post-monsoon period (negative soil moisture anomalies  
in October in Fig. 9d) in these climatologically dry western and peninsular Indian  
regions, mainly due to the cumulative effect of decreased rainfall during JJAS (see, for  
instance, the end of the black curve corresponding to west India in Fig. 4a). However,  
the southern tip of India shows elevated soil moisture in response to rainfall during  
the onset of the northeast monsoon in October when the east coast and peninsular  
India begin to receive rainfall. Finally, while most of India experiences severe soil stress  
(negative soil moisture anomalies), northeast India sees above normal soil moisture in  
response to increased JJAS rainfall.

In Type-2 droughts, even though central India and the Indo-Gangetic Plains region  
experience marginally decreased soil moisture in July, the deficit is mainly confined  
to Bundelkhand (Figs. 9e-h). Unlike in the Type-1 case, the west and Peninsular  
India regions show increased soil moisture availability in response to increased rain-  
fall during late July. Subsequently, the cumulative effect of rainfall distribution in the  
localised Type-2 drought becomes evident from August as parts of central India and  
Bundelkhand experience decreased soil moisture. In contrast, increased soil moisture  
persists in other regions of the country as they receive near-to-above-normal rainfall.  
Furthermore, the magnitude of soil moisture in Bundelkhand during Type-2 droughts  
is lesser than that during Type-1 droughts. As the season progresses into the month  
of October (i.e., post-monsoon), while Peninsular and west India region show signif-  
icantly increased soil moisture, the deficit remains localised to Bundelkhand. Thus,

875 in addition to rainfall evolution and its spatial extent, the spatial distribution of the  
876 soil moisture anomalies and their magnitude also serve as key differentiators between  
877 the two drought scenarios in a hydrological context, highlighting the need to consider  
878 these drought categories in a more holistic framework, for improved water management  
881 strategies.

883 Meteorological droughts also influence regional groundwater (GW) dynamics. Like  
884 soil moisture, the response of the regional groundwater to rainfall is also lagged, owing  
885 to the storage characteristics of the underlying aquifer. However, the sustained deple-  
886 tion of groundwater reserves in Bundelkhand is evident in the evolution of the depth  
887 to groundwater levels (Fig. 10) over the past two decades. Between 1995 and 2019,  
888 Bundelkhand experienced five Type-1 droughts (2002, 2004, 2009, 2014 and 2015)  
889 and four Type-2 droughts (2006, 2007, 2010 and 2017). The depletion in ground-  
890 water is particularly prominent during 2005 and 2009 (Fig. 10a) when the region  
891 experienced a meteorological drought nearly every year between 2004 and 2009. Dur-  
892 ing this period, the post-monsoon average depth to groundwater level decreased from  
893 5m before 2005 to almost 10m by the end of 2008, leading to a severe reduction in  
894 the available groundwater storage. Notably, northern Bundelkhand experiences more  
895 drawdown compared to the south; interestingly, this depletion appears to mirror the  
896 spatial heterogeneity in rainfall climatology between the northern and southern parts  
897 (see Fig. S1). This region also exhibits slower recovery post-2009, highlighting the  
898 compounding impact of frequent droughts in an arid situation. Further, a marginal  
899 decline in groundwater levels is observed between 2015 and 2018, coinciding with the  
900 three Type-2 droughts in 2014, 2015, and 2017. This pattern suggests that frequent  
901 meteorological droughts are plausible drivers of subsurface storage depletion in Bun-  
902 delkhand, potentially worsening water availability. However, the role of anthropogenic  
903 adaptations must be considered, particularly in a region like Bundelkhand, which lies  
904  
905  
906  
907  
908  
909  
910  
911  
912  
913  
914  
915  
916  
917  
918  
919  
920

in the Indo-Gangetic Plains, where agriculture is highly reliant on GW pumping ([Maurya et al., 2024](#)). Hence, the GW depletion in Bundelkhand is attributable to serial meteorological droughts compounded by concurrent human intervention.

## 4 Summary and Discussion

Over the last two decades, the decrease (increase) of summer monsoon rainfall over central India has manifested as a dipole pattern. Whether this recent decline in rainfall is only climate change related or a combination of secular changes with multidecadal variability still remains an open question. Even though previous studies have analysed droughts during year with a rainfall dipole, their subseasonal evolution has not been explored in detail. In this study, we analyse the June through September (JJAS) rainfall over the past century (1901 to 2023), and show that the rainfall deficit zone during these years of dipole is primarily localised over Bundelkhand, a water-scarce region in east-central India. Based on the spatio-temporal structure of rainfall, we categorised the droughts over Bundelkhand as Type-1 and Type-2. Type-1 droughts - coinciding for the most part with all-India droughts, are characterised by widespread rainfall deficit events encompassing both Bundelkhand and central India. On the other hand, during Type-2 droughts, rainfall deficit (excess) is highly localised to the Bundelkhand (west and peninsular India) region, resulting in what appears to be a prominent dipole pattern in rainfall.

Our analysis further reveals that the subseasonal spatial and temporal evolution of rainfall in these two droughts are distinctly different. In Type-1 droughts, rainfall deficit initially appears across central India and the western coast of India, starting in mid-June and is sustained throughout the JJAS season. In contrast, the rainfall deficit in Type-2 droughts initially develops across northeast India and Bundelkhand around mid-July. The magnitude of rainfall deficit (excess) peaks in Bundelkhand (west and peninsular India) during early August and sustains until early September, signifying

967 the subseasonal nature of the observed dipole pattern. Even though the subseasonal  
968 rainfall evolution differs between the two drought types, the final end-of-season rainfall  
969 deficit in Bundelkhand reaches a magnitude of approximately 300 mm in both cases  
970 (nearly 30-40% of the seasonal accumulation).

971  
972  
973       The contrasting spatio-temporal rainfall patterns between these droughts  
974 prompted us to analyse the atmospheric circulation. As Type-1 droughts are a subset  
975 of the classical ISMR droughts linked to ENSO, we primarily focussed on the less-  
976 studied Type-2 droughts. We observe that a midlatitude stationary Rossby wavetrain  
977 induces an anomalous anticyclone over western North Pacific between late July and  
978 mid-August. This anomalous anticyclone then drives easterlies over the South China  
979 Sea into east-central India, reducing the regional moisture influx from monsoon north-  
980 westerlies. During August, the midlatitude Rossby wavetrain migrates southwards to  
981 30°N and modulates an anomalous anticyclone over the Tibetan Plateau and along the  
982 Himalayan foothills. As a result, atmospheric subsidence over east-central India leads  
983 to decreased convection and rainfall. During September, the high-pressure region over  
984 Tibetan Plateau migrates further southward into central India, increasing (decreas-  
985 ing) subsidence (convection). The midlatitude westerly Rossby wavetrain also induces  
986 an anomalous cyclonic circulation over northwest India and Pakistan, increasing mois-  
987 ture convergence from the Arabian Sea, leading to increased convection (rainfall) over  
988 west India, thereby contributing to zonal asymmetry (dipole) in rainfall. In summary,  
989 a combined effect of intraseasonal variations in the midlatitude jet and the circulation  
990 over western North Pacific and Tibetan Plateau are responsible for the observed sum-  
991 mer monsoon rainfall dipole pattern. Having said that, further investigation is needed  
992 in this regard as a flood situation in northwest India and Pakistan induces strong dia-  
993 batic forcing, affecting the location of the crucial midlatitude jet ([Fu et al., 2024](#)). To  
994  
995  
996  
997  
998  
999  
1000  
1001  
1002  
1003  
1004  
1005  
1006  
1007  
1008  
1009  
1010  
1011  
1012

this end, the dynamics of the southward migration of the midlatitude jet on intraseasonal timescales, that induces a Tibetan high during Type-2 droughts, needs further investigation.

Apart from rainfall deficit, meteorological droughts also impact other critical variables within the local hydrological cycle at the downstream end. Specifically, during Type-1 droughts, we find large-scale deficit in soil moisture across central and peninsular India during the peak monsoon months of July and August, persisting into the post-monsoon season. Type-2 droughts, on the other hand, exhibit more localised deficit in soil moisture, which in fact is confined to Bundelkhand (providing yet another distinct difference between the two kinds of droughts). Furthermore, we find that the enhanced soil stress (dryness) owing to reduced rain may have a role to play in the much-reported depletion of groundwater storage in northwest India in general ([Rodell et al., 2009](#); [Bhanja et al., 2016](#)) and Bundelkhand in particular (over and above human intervention), especially in the recent twenty years. Consequently, both Type-1 and Type-2 droughts significantly threaten agricultural yields in Bundelkhand due to sustained soil moisture deficit and diminishing groundwater availability.

In the Indo-Gangetic plains, where the columnar water vapour has comparable contributions from moisture convergence and local evapotranspiration, the regional soil moisture has the potential to modulate local rainfall patterns through positive or negative feedback pathways ([Yeh et al., 1984](#); [Varikoden and Revadekar, 2018](#); [Qing et al., 2023](#)). If positive feedback occurs between rainfall and soil moisture, Type-2 droughts could further decrease (increase) the availability of atmospheric moisture for rainfall in Bundelkhand (western India). Indeed, recent studies document significant increases in precipitation and moisture availability driving widespread greening in parts of Western India, such as the Thar Desert ([Kashyap et al., 2025](#); [Mishra et al., 2025](#)). Interestingly, this greening is sustained not only by enhanced rainfall but also significantly by groundwater extraction, highlighting the complex interplay between

1059 climatic shifts and hydrological management in the region ([Mishra et al., 2025](#)). On  
1060 the other hand, it is plausible that if there is a negative feedback between rainfall  
1061 and soil moisture, increased soil moisture might not result in increased local rainfall  
1062  
1063 over western India. Thus, investigating the soil moisture-atmosphere interactions dur-  
1064 ing Type-2 droughts would be essential to further advance our understanding of the  
1065 physical mechanisms involved in these feedback loops.  
1066

1067 The findings presented here have important implications for drought management  
1068 in Bundelkhand (and Indo-Gangetic Plains). Any anthropogenic activities, such as  
1069 increased groundwater pumping for agriculture, could only serve to aggravate water  
1070 scarcity concerns. Further depletion of groundwater resources could trigger a positive  
1071 feedback loop: declining soil moisture, coupled with reduced evapotranspiration, can  
1072 decrease atmospheric moisture availability, increasing the risk of localised droughts.  
1073  
1074 Further investigations into local groundwater flow, recharge, and evapotranspiration  
1075 patterns are thus crucial. Finally, drought mitigation strategies for Bundelkhand must  
1076 be informed by the distinct vulnerabilities associated with both Type-1 and Type-2  
1077 droughts.  
1078

1079

1080

1081

1082

1083

1084 droughts.

1085

1086

1087

1088

1089

1090

1091

1092

1093

1094

1095

1096

1097

1098

1099

1100

1101

1102

1103

1104

Drought Year	Bundelkhand		
	$D_i$	$Z_i$	
1905	-28.77	-1.67	1105
1907	-24.46	-1.38	1106
1913	-30.11	-1.74	1107
1918	-35.20	-1.42	1108
1928	-32.62	-1.44	1109
1941	-30.12	-1.74	1110
1965	-34.31	-1.99	1111
1966	-23.31	-1.35	1112
1979	-40.06	-2.32	1113
1989	-19.61	-1.13	1114
2002	-19.75	-1.14	1115
2004	-20.03	-1.16	1116
2006	-31.21	-1.81	1117
2007	-29.67	-1.72	1118
2009	-35.62	-2.06	1119
2010	-19.64	-1.14	1120
2014	-33.20	-1.92	1121
2015	-34.30	-1.99	1122
2017	-28.04	-1.62	1123
2020	-17.93	-1.04	1124
			1125
			1126
			1127
			1128
			1129
			1130
			1131
			1132
			1133
			1134
			1135
			1136
			1137
			1138
			1139
			1140
			1141
			1142
			1143
			1144
			1145
			1146
			1147
			1148
			1149
			1150

**Table 1:** Percentage seasonal (June - September) rainfall deviation ( $D_i$ ) and normalized JJAS rainfall deviations ( $Z_i$ ) from the long-term mean for all drought years in Bundelkhand. See Eqn. (3).

1151	Drought Year	Rainfall Anomaly (%)	
		Bundelkhand	AISMR
1152	1905	-29	-16
1153	1907	-24	-9
1154	1913	-30	-8
1155	1918	-35	-24
1156	1928	-33	-10
1157	1941	-30	-15
1158	1965	-34	-17
1159	1966	-23	-13
1160	1979	-40	-17
1161	1989	-20	2
1162	2002	-20	-22
1163	2004	-20	-13
1164	2006	-31	2
1165	2007	-30	10
1166	2009	-36	-22
1167	2010	-20	-1
1168	2014	-33	-14
1169	2015	-34	-14
1170	2017	-28	-5
1171	2020	-18	9

**Table 2:** Seasonal (June - September) rainfall deviation from long-term mean for Bundelkhand and all India, as a % (Eqn. 3), for each drought year shown in red for Type-1 and blue for Type-2 droughts. These values form the basis for Fig. 2.

1176  
1177  
1178  
1179  
1180  
1181  
1182  
1183  
1184  
1185  
1186  
1187  
1188  
1189  
1190  
1191  
1192  
1193  
1194  
1195  
1196

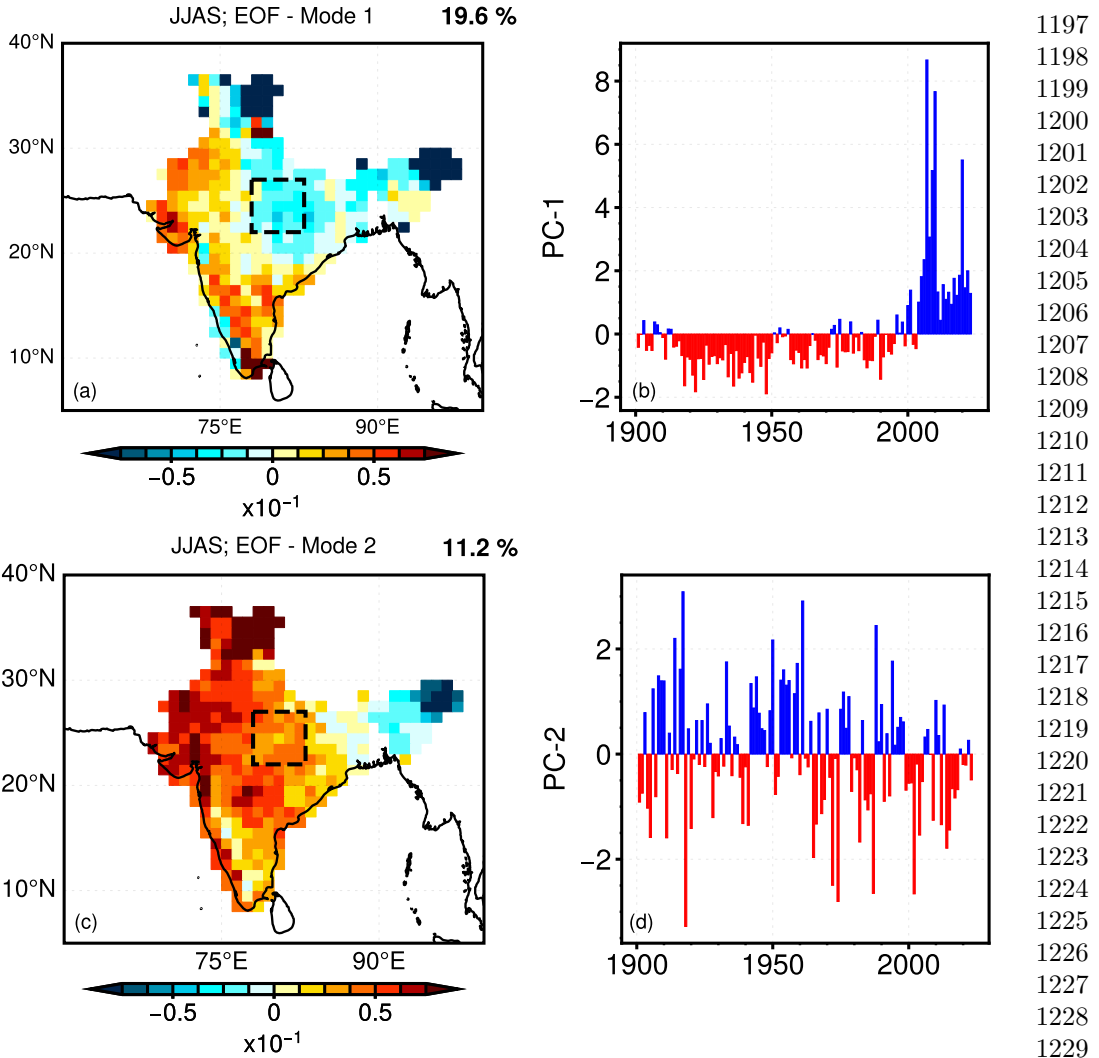


**Fig. 1:** The first two modes of an Empirical Orthogonal Function (EOF) analysis of interannual JJAS rainfall (normalised; see Appendix A) during 1901-2023. (a,c) EOFs and (b, d) corresponding principal components. The region inside the dashed rectangle represents Bundelkhand ( $22\text{-}27^\circ\text{N}$ ,  $78\text{-}83^\circ\text{E}$ ; see also Fig. S1). Based on IMD 1-degree, daily rainfall for 1901-2023.

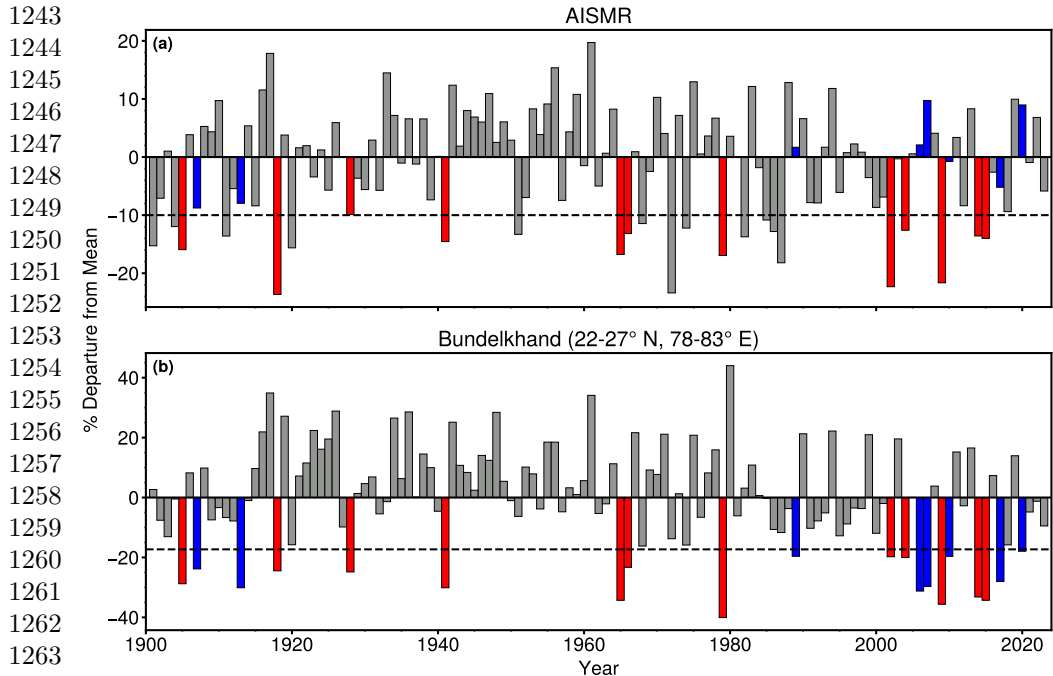


**Fig. 2:** Long-term variation of (a) all-India and (b) Bundelkhand summer monsoon rainfall anomalies, shown as a departure (in %) from long-term mean. As per the India Meteorological Department (IMD), a year is classified as a drought if the seasonal deficit is more than 1 interannual standard deviation. In terms of % departure from the long-term mean, this translates to  $\approx 10\%$  for India as a whole and  $\approx 17\%$  for Bundelkhand, a smaller region (shown as dashed horizontal lines in both panels; see also Tables 1 and 2). The red and blue bars denote Type-1 (common to both regions) and Type-2 (specific to Bundelkhand) droughts. Based on IITM homogeneous monthly rainfall and IMD 1-degree, daily rainfall for 1901-2023.

1274  
1275  
1276  
1277  
1278  
1279  
1280  
1281  
1282  
1283  
1284  
1285  
1286  
1287  
1288

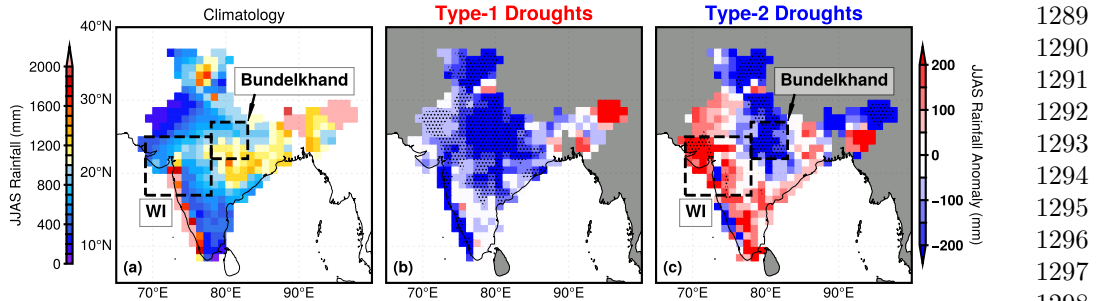


**Fig. 3:** Spatial distribution of June-September rainfall (a) climatology for 1901-2023; and (b, c) anomalies for Type-1 and Type-2 drought composites, respectively. The smaller and larger rectangles denote Bundelkhand and West India (WI) respectively. Stippling indicates regions where the anomalies are statistically significant at the 95% confidence level based on a two-sided Student's t-test. Based on IMD 1-degree, daily rainfall for 1901-2023.

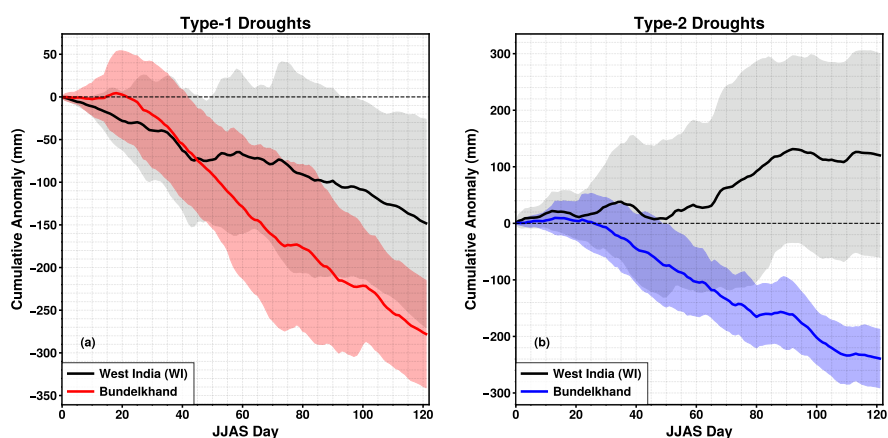
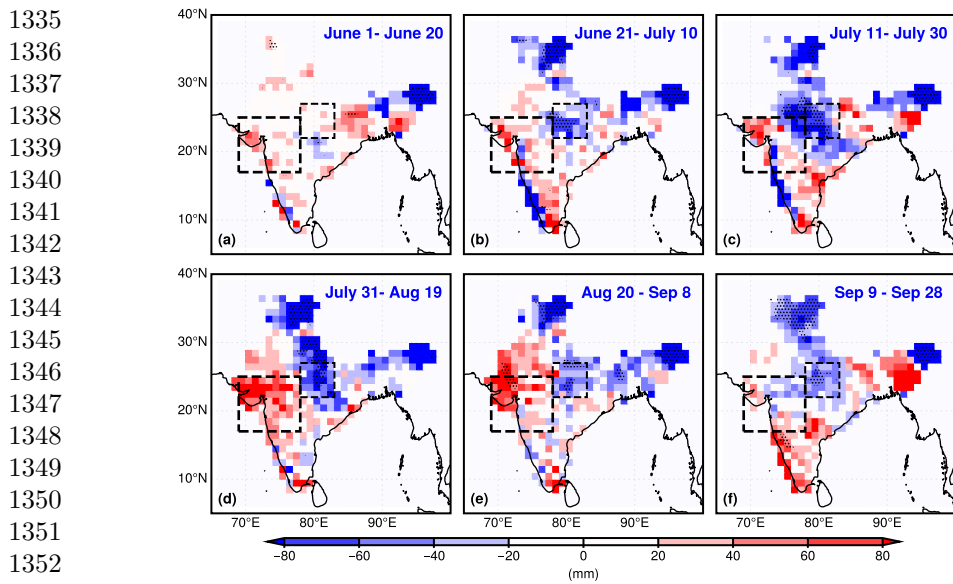


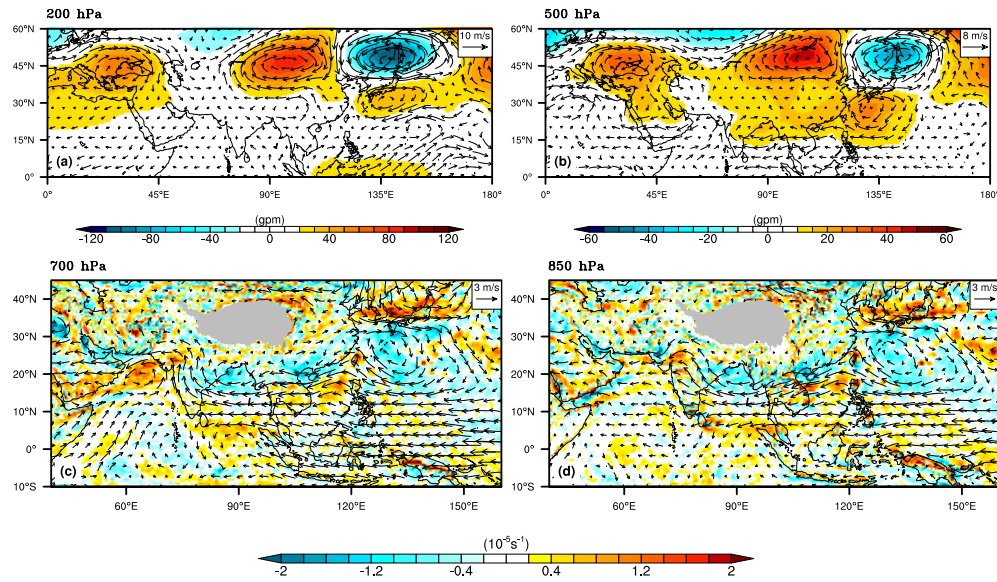
**Fig. 4:** Composite of the cumulative of daily area-averaged rainfall anomalies (mm) for Bundelkhand and western India regions during (a) Type-1 and (b) Type-2 droughts. The solid lines denote the mean cumulative anomaly, and the shading represents  $\pm 1$  standard deviation, estimated from 12 Type-1 and 8 Type-2 drought years. Based on IMD 1-degree, daily rainfall for 1901-2023.

1289  
1290  
1291  
1292  
1293  
1294  
1295  
1296  
1297  
1298  
1299  
1300  
1301  
1302  
1303  
1304  
1305  
1306  
1307  
1308  
1309  
1310  
1311  
1312  
1313  
1314  
1315  
1316  
1317  
1318  
1319  
1320  
1321  
1322  
1323  
1324  
1325  
1326  
1327  
1328  
1329  
1330  
1331  
1332  
1333  
1334



1335  
1336  
1337  
1338  
1339  
1340  
1341  
1342  
1343  
1344  
1345  
1346  
1347  
1348  
1349  
1350  
1351  
1352  
1353 **Fig. 5:** Spatial distribution of cumulative rainfall anomalies over a 20-day timescale for  
1354 Type-2 droughts. The large and small rectangles denote west India and Bundelkhand  
1355 regions, respectively. Stippling indicates regions where the anomalies are statistically  
1356 significant at the 95% confidence level following a two-sided Student's t-test. Based  
1357 on IMD 1-degree, daily rainfall for 1901-2023.  
1358  
1359  
1360  
1361  
1362  
1363  
1364  
1365  
1366  
1367  
1368  
1369  
1370  
1371  
1372  
1373  
1374  
1375  
1376  
1377  
1378  
1379  
1380

### Type - 2 Droughts : July 20-31



### Type - 2 Droughts : August 1 - August 15

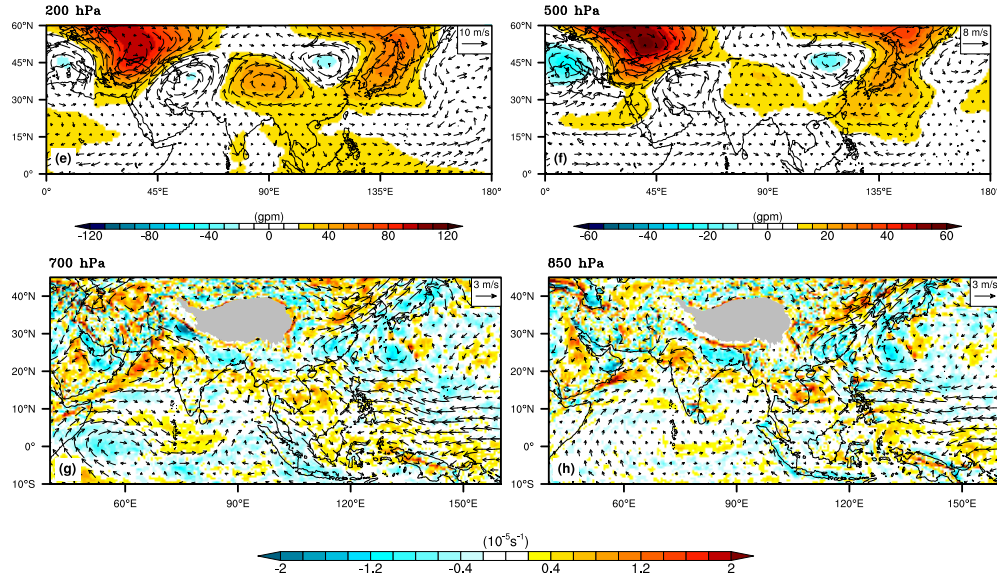


**Fig. 6:** Type-2 drought composites for the periods July 20-31 and August 1-15: (a, b, e, f) Geopotential Height (gpm; shading) and wind anomalies (vectors) at 200 and 500 hPa. (c, d, g, h) wind anomalies (vectors) and relative vorticity ( $10^{-5} s^{-1}$ ; shading) at 700 and 850 hPa. Only the five most recent Type-2 drought years were included in the composites. The shading in grey (in panels c, d, g and h) denotes the Tibetan Plateau. Based on ERA5 0.25-degree, daily reanalysis data for 1970-2023.

1381  
1382  
1383  
1384  
1385  
1386  
1387  
1388  
1389  
1390  
1391  
1392  
1393  
1394  
1395  
1396  
1397  
1398  
1399  
1400  
1401  
1402  
1403  
1404  
1405  
1406  
1407  
1408  
1409  
1410  
1411  
1412  
1413  
1414  
1415  
1416  
1417  
1418  
1419  
1420  
1421  
1422  
1423  
1424  
1425  
1426

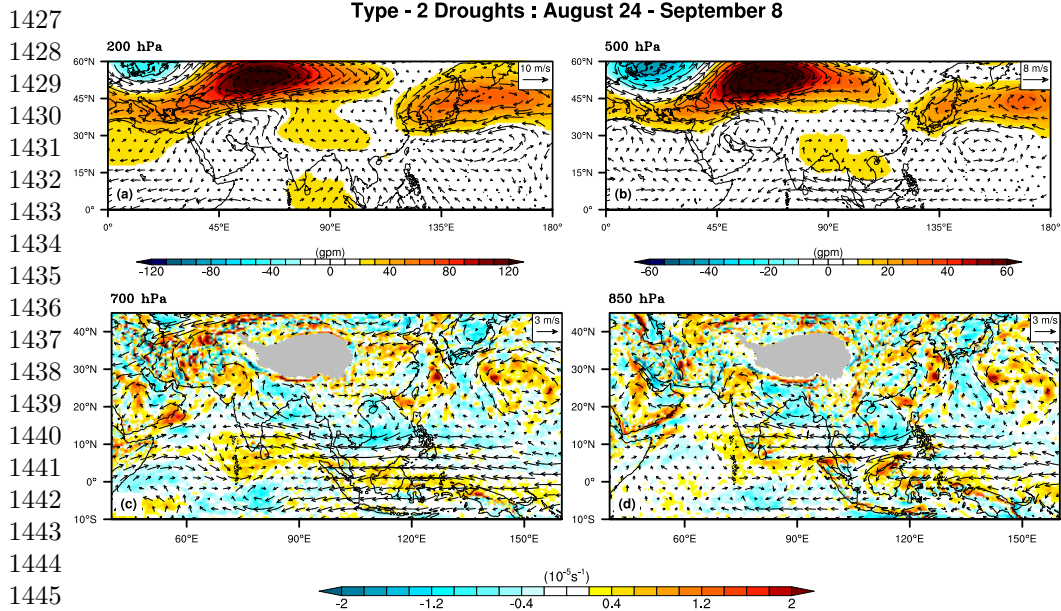


**Fig. 7:** Same as in Fig. 6, but for the period August 24 - September 8.

1427  
1428  
1429  
1430  
1431  
1432  
1433  
1434  
1435  
1436  
1437  
1438  
1439  
1440  
1441  
1442  
1443  
1444  
1445  
1446  
1447  
1448  
1449  
1450  
1451  
1452  
1453  
1454  
1455  
1456  
1457  
1458  
1459  
1460  
1461  
1462  
1463  
1464  
1465  
1466  
1467  
1468  
1469  
1470  
1471  
1472

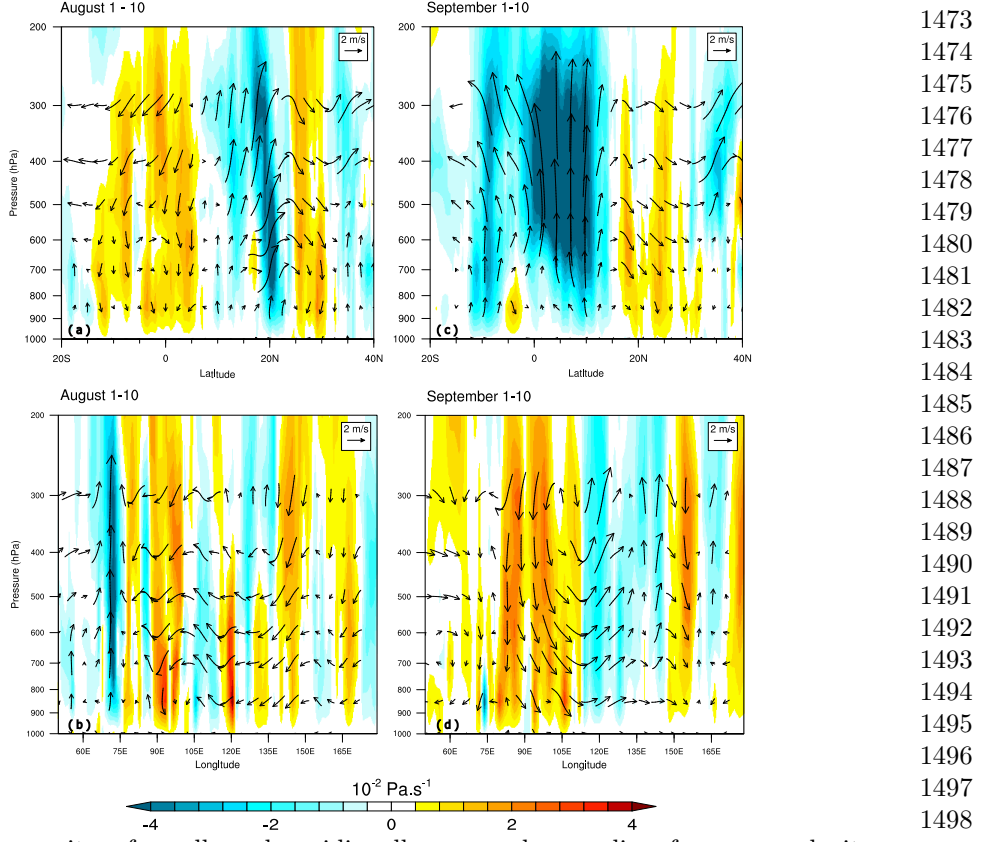
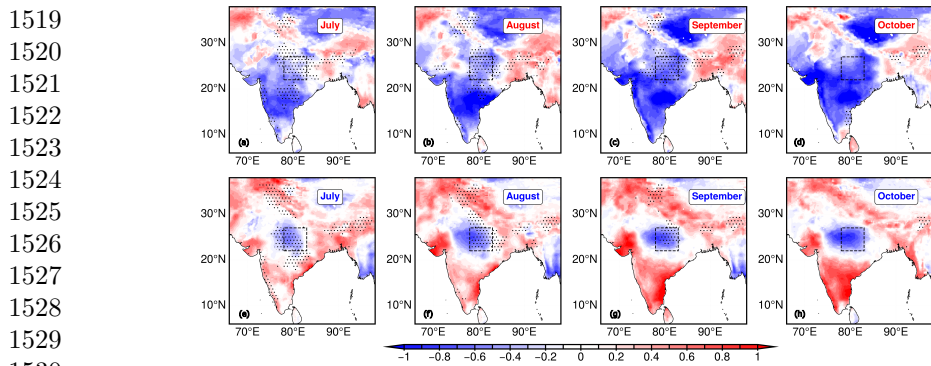
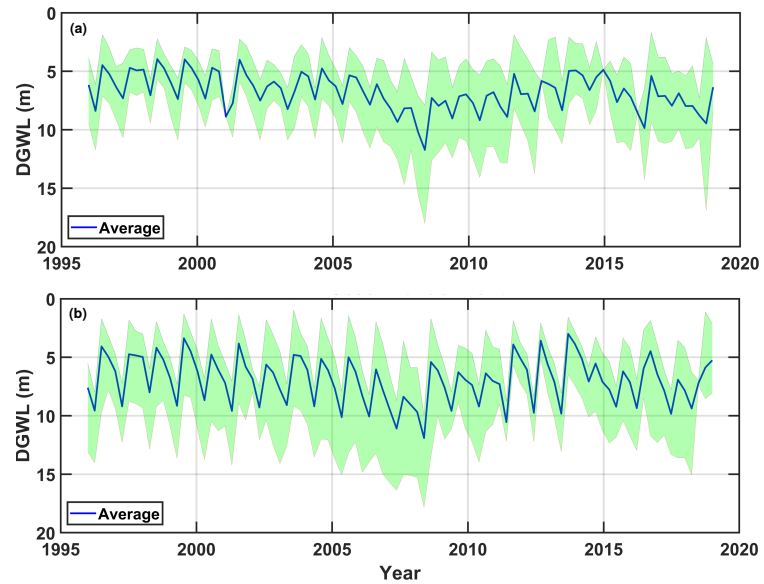


**Fig. 8:** Composites of zonally and meridionally averaged anomalies of pressure velocity ( $\omega$ ; shading) and wind (vectors) during Type-2 droughts for (left column) August 1–10 and (right column) September 1–10. (a, c) Meridional-vertical and (b, d) Zonal-vertical cross-sections. The zonal and meridional averages are computed over  $69^{\circ}\text{E}$ – $83^{\circ}\text{E}$  and over  $17^{\circ}\text{N}$ – $27^{\circ}\text{N}$ , respectively. Only the five most recent Type-2 drought years were included in the composites. The vertical velocity ( $w$ ) used for the wind vectors has been scaled by  $10^3$  for ease of visualisation. Based on ERA5 0.25-degree, daily reanalysis data for 1970–2023.



1519  
1520  
1521  
1522  
1523  
1524  
1525  
1526  
1527  
1528  
1529  
1530  
1531 **Fig. 9:** Normalised soil moisture anomalies for (top row; a-d) Type-1 and (bottom row;  
1532 e-h) Type-2 drought composites from July till October. Regions with rainfall deficit  
1533 ( $\leq -1$  mm/day) during the same month are hatched. The normalised anomalies are  
1534 estimated as was done for rainfall. The dashed box denotes Bundelkhand. Based on  
1535 GLDAS 0.25-degree, daily soil moisture and IMD 0.25-degree, daily rainfall data for  
1536 2003-2023.  
1537  
1538  
1539  
1540  
1541



1542  
1543  
1544  
1545  
1546  
1547  
1548  
1549  
1550  
1551  
1552  
1553  
1554  
1555  
1556  
1557  
1558  
1559  
1560 **Fig. 10:** Time series of depth to groundwater level (DGWL; m) in (a) northern and  
1561 (b) southern Bundelkhand. The blue line represents the mean, and green shading  
1562 represents minimum and maximum DGWL. Based on Central Ground Water Board  
1563 (CGWB) well data for 1995-2019.  
1564

<b>References</b>	1565
Ashok K, Guan Z, Yamagata T (2001) Impact of the Indian Ocean dipole on the relationship between the Indian monsoon rainfall and ENSO. <i>Geophysical Research Letters</i> 28(23):4499–4502. <a href="https://doi.org/10.1029/2001GL013294">https://doi.org/10.1029/2001GL013294</a>	1566
Athira KS, Roxy MK, Dasgupta P, et al. (2023) Regional and temporal variability of Indian summer monsoon rainfall in relation to El Niño southern oscillation. <i>Scientific Reports</i> 13(1):12643. <a href="https://doi.org/10.1038/s41598-023-38730-5">https://doi.org/10.1038/s41598-023-38730-5</a>	1567
Behera SK, Ratnam JV (2018) Quasi-asymmetric response of the indian summer monsoon rainfall to opposite phases of the iod. <i>Scientific Reports</i> 8(1):123. <a href="https://doi.org/10.1038/s41598-017-18396-6">https://doi.org/10.1038/s41598-017-18396-6</a>	1568
Bhanja SN, Mukherjee A, Dipankar, et al. (2016) Validation of GRACE based groundwater storage anomaly using in-situ groundwater level measurements in India. <i>Journal of Hydrology</i> 543:729–738. <a href="https://doi.org/10.1016/j.jhydrol.2016.10.042">https://doi.org/10.1016/j.jhydrol.2016.10.042</a>	1569
Boers N, Goswami B, Rheinwalt A, et al. (2019) Complex networks reveal global pattern of extreme-rainfall teleconnections. <i>Nature</i> 566(7744):373–377. <a href="https://doi.org/10.1038/s41586-018-0872-x">https://doi.org/10.1038/s41586-018-0872-x</a>	1570
Borah PJ, Venugopal V, Sukhatme J, et al. (2020) Indian monsoon derailed by a north atlantic wavetrain. <i>Science</i> 370(6522):1335–1338. <a href="https://doi.org/10.1126/science.aay6043">https://doi.org/10.1126/science.aay6043</a>	1571
Chaluvadi R, Varikoden H, Mujumdar M, et al. (2024) The combined influence of west Pacific subtropical high and tropical cyclones over the northwest Pacific on Indian summer monsoon rainfall. <i>Quarterly Journal of the Royal Meteorological Society</i> 150(759):1157–1171. <a href="https://doi.org/10.1002/qj.4640">https://doi.org/10.1002/qj.4640</a> , <a href="https://rmets.onlinelibrary.wiley.com/doi/pdf/10.1002/qj.4640">https://rmets.onlinelibrary.wiley.com/doi/pdf/10.1002/qj.4640</a>	1572

1611 Darshana P, Chowdary JS, Gnanaseelan C, et al. (2020) Interdecadal modulation of  
1612 the Indo-western Pacific Ocean Capacitor mode and its influence on Indian sum-  
1613 mer monsoon rainfall. Climate Dynamics 54(3):1761–1777. <https://doi.org/10.1007/s00382-019-05085-5>  
1617  
1618 Deng K, Yang S, Ting M, et al. (2019) Dominant modes of China summer heat  
1619 waves driven by global sea surface temperature and atmospheric internal variability.  
1620 Journal of Climate 32(12):3761–3775. <https://doi.org/10.1175/JCLI-D-18-0256.1>  
1623  
1624 Fu ZH, Zhou W, Xie SP, et al. (2024) Dynamic pathway linking Pakistan flooding  
1625 to East Asian heatwaves. Science Advances 10(17):9250. <https://doi.org/10.1126/sciadv.adk9250>  
1628  
1629  
1630 Gadgil S, Gadgil S (2006) The Indian Monsoon, GDP and Agriculture. Economic and  
1631 Political Weekly 41(47):4887–4895. URL <http://www.jstor.org/stable/4418949>  
1633  
1634 Gadgil S, Vinayachandran PN, Francis PA, et al. (2004) Extremes of the indian sum-  
1635 mer monsoon rainfall, enso and equatorial indian ocean oscillation. Geophysical  
1636 Research Letters 31(12). <https://doi.org/10.1029/2004GL019733>  
1638  
1639  
1640 Gadgil S, Cane MA, Francis P (2023) On rogue La Niñas, with below-average mon-  
1641soon rainfall. Journal of Earth System Science 132(3):111. <https://doi.org/10.1007/s12040-023-02121-1>  
1644  
1645  
1646 Goswami BB (2023) Role of the eastern equatorial Indian Ocean warming in the  
1647 Indian summer monsoon rainfall trend. Climate Dynamics 60(1):427–442. <https://doi.org/10.1007/s00382-022-06337-7>  
1649  
1650  
1651  
1652 Goswami BN (1998) The physics of ENSO-monsoon connection. Indian Journal of  
1653 Marine Sciences 27:82–89. URL <http://nopr.niscpr.res.in/handle/123456789/35741>  
1655  
1656

Goswami BN, Venugopal V, Sengupta D, et al. (2006) Increasing Trend of Extreme Rain Events Over India in a Warming Environment. <i>Science</i> 314(5804):1442–1445.	1657 1658 1659 1660 1661 1662 1663 1664 1665 1666 1667 1668 1669 1670 1671 1672 1673 1674 1675 1676 1677 1678 1679 1680 1681 1682 1683 1684 1685 1686 1687 1688 1689 1690 1691 1692 1693 1694 1695 1696 1697 1698 1699 1700 1701 1702
<a href="https://doi.org/10.1126/science.1132027">https://doi.org/10.1126/science.1132027</a>	
Jiang X, Ting M (2017) A dipole pattern of summertime rainfall across the Indian subcontinent and the Tibetan Plateau. <i>Journal of Climate</i> 30(23):9607–9620. <a href="https://doi.org/10.1175/JCLI-D-16-0914.1">https://doi.org/10.1175/JCLI-D-16-0914.1</a>	
Kashyap R, Kuttippurath J, and VKP (2025) Agriculture intensification and moisture-induced Thar desert greening: implications for energy balance, socio-economy, and biodiversity. <i>GIScience &amp; Remote Sensing</i> 62(1):2483458. <a href="https://doi.org/10.1080/15481603.2025.2483458">https://doi.org/10.1080/15481603.2025.2483458</a>	
Kennedy JJ, Rayner NA, Atkinson CP, et al. (2019) An ensemble data set of sea surface temperature change from 1850: The met office hadley centre hadsst.4.0.0.0 data set. <i>Journal of Geophysical Research: Atmospheres</i> 124(14):7719–7763. <a href="https://doi.org/10.1029/2018JD029867">https://doi.org/10.1029/2018JD029867</a>	
Kiran Kumar P, Singh A (2021) Increase in summer monsoon rainfall over the north-east India during El Niño years since 1600. <i>Climate Dynamics</i> 57(3):851–863. <a href="https://doi.org/10.1007/s00382-021-05743-7">https://doi.org/10.1007/s00382-021-05743-7</a>	
Krishnamurthy V, Goswami BN (2000) Indian monsoon–ENSO relationship on interdecadal timescale. <i>Journal of Climate</i> 13(3):579–595. <a href="https://doi.org/10.1175/1520-0442(2000)013&lt;0579:IMEROI&gt;2.0.CO;2">https://doi.org/10.1175/1520-0442(2000)013&lt;0579:IMEROI&gt;2.0.CO;2</a>	
Li B, Beaudoing H, Rodell M (2020) GLDAS Catchment Land Surface Model L4 Daily 0.25 × 0.25 Degree GRACE-DA1 V2. 2, Greenbelt, Maryland, USA. Goddard Earth Sciences Data and Information Services Center (GES DISC) <a href="https://doi.org/10.5067/LYHA9088MFWQ">https://doi.org/10.5067/LYHA9088MFWQ</a>	

1703 Maurya AK, Swarnkar S, Prakash S (2024) Hydrological impacts of altered monsoon  
1704 rain spells in the Indian Ganga basin: a century-long perspective. Environmental  
1705 Research: Climate 3(1):015010. <https://doi.org/10.1088/2752-5295/ad34a9>  
1706  
1707  
1708  
1709 Mishra V, Smoliak BV, Lettenmaier DP, et al. (2012) A prominent pattern of year-to-  
1710 year variability in Indian Summer Monsoon Rainfall. Proceedings of the National  
1711 Academy of Sciences 109(19):7213–7217. <https://doi.org/10.1073/pnas.1119150109>  
1712  
1713  
1714  
1715 Mishra V, Solanki H, Nemani R (2025) Greening of the thar desert driven by climate  
1716 change and human interventions. Cell Reports Sustainability p 100364. <https://doi.org/10.1016/j.crsus.2025.100364>  
1716  
1717  
1718  
1719  
1720 Mooley D, Parthasarathy B (1983) Indian summer monsoon and El Niño. Pure and  
1721 Applied Geophysics 121:339–352. <https://doi.org/10.1007/BF02590143>  
1722  
1723  
1724 Pai D, Sridhar L, Ramesh Kumar M (2016) Active and break events of Indian summer  
1725 monsoon during 1901–2014. Climate Dynamics 46:3921–3939. <https://doi.org/10.1007/s00382-015-2813-9>  
1726  
1727  
1728  
1729  
1730 Parthasarathy B, Mooley D (1978) Some features of a long homogeneous series of  
1731 Indian summer monsoon rainfall. Monthly Weather Review 106(6):771–781. [https://doi.org/10.1175/1520-0493\(1978\)106<771:SFOALH>2.0.CO;2](https://doi.org/10.1175/1520-0493(1978)106<771:SFOALH>2.0.CO;2)  
1732  
1733  
1734  
1735  
1736 Parthasarathy B, Munot A, Kothawale D (1994) All-India monthly and seasonal  
1737 rainfall series: 1871–1993. Theoretical and Applied Climatology 49:217–224. <https://doi.org/10.1007/BF00867461>  
1738  
1739  
1740  
1741  
1742 Patidar R, Pingale SM, Khare D, et al. (2024) Spatio-temporal assessment of multi-  
1743 scalar meteorological and hydrological droughts over Bundelkhand, India. Physics  
1744 and Chemistry of the Earth, Parts A/B/C 136:103729. <https://doi.org/10.1016/j.pce.2024.103729>  
1745  
1746  
1747  
1748

- Qing Y, Wang S, Yang ZL, et al. (2023) Soil moisture atmosphere feedbacks have triggered the shifts from drought to pluvial conditions since 1980. *Communications Earth and Environment* 4(1):254. <https://doi.org/10.1038/s43247-023-00922-2> 1749  
 1750  
 1751  
 1752  
 1753  
 1754  
 1755  
 1756  
 1757  
 1758  
 1759  
 1760  
 1761  
 1762  
 1763  
 1764  
 1765  
 1766  
 1767  
 1768  
 1769  
 1770  
 1771  
 1772  
 1773  
 1774  
 1775  
 1776  
 1777  
 1778  
 1779  
 1780  
 1781  
 1782  
 1783  
 1784  
 1785  
 1786  
 1787  
 1788  
 1789  
 1790  
 1791  
 1792  
 1793  
 1794
- Rajagopalan B, Molnar P (2013) Signatures of Tibetan Plateau heating on Indian summer monsoon rainfall variability. *Journal of Geophysical Research: Atmospheres* 118(3):1170–1178. <https://doi.org/10.1002/jgrd.50124>
- Rajeevan M, Sridhar L (2008) Inter-annual relationship between Atlantic sea surface temperature anomalies and Indian summer monsoon. *Geophysical Research Letters* 35(21). <https://doi.org/10.1029/2008GL036025>
- Rajeevan M, Bhate J, Kale J, et al. (2006) High resolution daily gridded rainfall data for the Indian region: Analysis of break and active monsoon spells. *Current Science* 91(3):296–306. URL [https://repository.ias.ac.in/94353/1/high\\_resolution.pdf](https://repository.ias.ac.in/94353/1/high_resolution.pdf)
- Rasmusson EM, Carpenter TH (1983) The relationship between eastern equatorial Pacific sea surface temperatures and rainfall over India and Sri Lanka. *Monthly Weather Review* 111(3):517–528. [https://doi.org/10.1175/1520-0493\(1983\)111<517:TRBE>2.0.CO;2](https://doi.org/10.1175/1520-0493(1983)111<517:TRBE>2.0.CO;2)
- Ratna BS, Sabeerali C, Sharma T, et al. (2024) Combined influence of el niño, iod and mjo on the indian summer monsoon rainfall: Case study for the years 1997 and 2015. *Atmospheric Research* 299:107214. <https://doi.org/10.1016/j.atmosres.2023.107214>
- Rodell M, Velicogna I, Famiglietti J (2009) Satellite-based estimates of groundwater depletion in India. *Nature* 460:999–1002. <https://doi.org/10.1038/nature08238>
- Roxy MK, Ritika K, Terray P, et al. (2015) Drying of Indian subcontinent by rapid Indian Ocean warming and a weakening land-sea thermal gradient. *Nature Communications* 6(1):7423. <https://doi.org/10.1038/ncomms8423>

1795 Roxy MK, Ghosh S, Pathak A, et al. (2017) A threefold rise in widespread extreme  
1796 rain events over central India. *Nature Communications* 8(1):1–11. <https://doi.org/10.1038/s41467-017-00744-9>  
1797  
1798  
1799  
1800  
1801 Saha P, Mahanta R, Rajesh P, et al. (2023) Persistent wet and dry spells of Indian  
1802 summer monsoon rainfall: A reexamination of definitions of “active” and “break”  
1803 events. *Journal of Climate* 36(1):261–277. <https://doi.org/10.1175/JCLI-D-21-1003.1>  
1804  
1805  
1806 1  
1807  
1808 Saikranthi K, Radhakrishna B, Satheesh S, et al. (2018) Spatial variation of different  
1809 rain systems during El Niño and La Niña periods over India and adjoining ocean.  
1810  
1811  
1812 Climate Dynamics 50:3671–3685. <https://doi.org/10.1007/s00382-017-3833-4>  
1813  
1814 Sharma A (2023) Rainfall deficiency, drought and economic growth in the Bundelk-  
1815 hand region of India. *Sustainable Water Resources Management* 9(3):72. <https://doi.org/10.1007/s40899-023-00851-0>  
1816  
1817  
1818  
1819  
1820 Sharma T, Satyaban B, Pai DS, et al. (2024) Indian summer monsoon rainfall response  
1821 to two distinct evolutions of La Niña events. *International Journal of Climatology*  
1822 44(12):4405–4427. <https://doi.org/10.1002/joc.8588>  
1823  
1824  
1825  
1826 Singh R, Jaiswal N, Kishtawal C (2022) Rising surface pressure over Tibetan Plateau  
1827 strengthens indian summer monsoon rainfall over northwestern India. *Scientific*  
1828  
1829 Reports 12(1):8621. <https://doi.org/10.1038/s41598-022-12523-8>  
1830  
1831  
1832 Soci C, Hersbach H, Simmons A, et al. (2024) The ERA5 global reanalysis from 1940  
1833 to 2022. *Quarterly Journal of the Royal Meteorological Society* 150(764):4014–4048.  
1834  
1835 <https://doi.org/10.1002/qj.4803>  
1836  
1837 Timmermann A, Soon-Il A, Kug JS, et al. (2018) El Niño–southern oscillation  
1838 complexity. *Nature* 559(7715):535–545. <https://doi.org/10.1038/s41586-018-0252-6>  
1839  
1840

- Varikoden H, Revadekar J (2018) Relation between the rainfall and soil moisture during different phases of Indian monsoon. *Pure and Applied Geophysics* 175:1187–1196. <https://doi.org/10.1007/s00024-017-1740-6> 1841  
 Webster PJ, Magaña VO, Palmer TN, et al. (1998) Monsoons: Processes, predictability, and the prospects for prediction. *Journal of Geophysical Research: Oceans* 103(C7):14451–14510. <https://doi.org/10.1029/97JC02719> 1842  
 Yadav R (2009) Role of equatorial central Pacific and northwest of North Atlantic 2-metre surface temperatures in modulating Indian summer monsoon variability. *Climate Dynamics* 32(4):549–563. <https://doi.org/10.1007/s00382-008-0410-x> 1843  
 Yeh TC, Wetherald RT, Manabe S (1984) The effect of soil moisture on the short-term climate and hydrology change—A numerical experiment. *Monthly Weather Review* 112(3):474–490. [https://doi.org/10.1175/1520-0493\(1984\)112<474:TEOSMO>2.0.CO;2](https://doi.org/10.1175/1520-0493(1984)112<474:TEOSMO>2.0.CO;2) 1844  
 Zhu Y, Liu Y, Wang W, et al. (2021) A global perspective on the probability of propagation of drought: From meteorological to soil moisture. *Journal of Hydrology* 603:126907. <https://doi.org/10.1016/j.jhydrol.2021.126907> 1845  
 1846  
 1847  
 1848  
 1849  
 1850  
 1851  
 1852  
 1853  
 1854  
 1855  
 1856  
 1857  
 1858  
 1859  
 1860  
 1861  
 1862  
 1863  
 1864  
 1865  
 1866  
 1867  
 1868  
 1869  
 1870  
 1871  
 1872  
 1873  
 1874  
 1875  
 1876  
 1877  
 1878  
 1879  
 1880  
 1881  
 1882  
 1883  
 1884  
 1885  
 1886

1887 **Acknowledgements.** The authors gratefully acknowledge the India Meteorological  
1888 Department (IMD) for providing access to gridded rainfall observation datasets. We  
1889 also acknowledge the use of ERA5 atmospheric reanalysis data, made available by the  
1890  
1891 Copernicus Climate Change Service (C3S) (<https://cds.climate.copernicus.eu/>).  
1892  
1893

1894 This research was conducted as part of the first author's doctoral dissertation. C.  
1895 Sarat gratefully acknowledges financial support from the Prime Minister's Research  
1896 Fellowship (PMRF), Government of India. C. Sarat also acknowledges the use of  
1897 Python programming language and the NCAR Command Language (NCL) (<https://www.ncl.ucar.edu/>) for data analysis and visualization.  
1898  
1899  
1900  
1901  
1902

## 1903 **Declarations**

1904  
1905

1906 **Conflict of Interest.** The authors declare that they have no conflicts of interest.  
1907

1908 **Data Availability.** All data used in this study are publicly available; repository  
1909 links have been provided where applicable. Python and NCL scripts developed for the  
1910 analysis are available from the corresponding author upon reasonable request.  
1911  
1912

1913 **Funding.** V. Venugopal acknowledges financial support from two sources: the Sci-  
1914 ence and Engineering Research Board (SERB), Department of Science and Technology,  
1915 1916 Govt. of India via grant number CRG/2021/002441; and Ministry of Earth Sciences  
1917 1918 (MoES), Govt. of India via IITM/MM-III/2024/IND-10, as part of Monsoon Mission  
1919 1920 Phase III.  
1921

1922 **Author Contributions.** Conceptualization: C. Sarat, V. Venugopal; Methodology:  
1923  
1924 C. Sarat, V. Venugopal; Formal analysis and investigation: C. Sarat; Writing – original  
1925  
1926 draft: C. Sarat; Writing – review and editing: C. Sarat, V. Venugopal, and Sekhar  
1927 Muddu.  
1928

1929

1930

1931

1932

1933  
1934  
1935  
1936  
1937  
1938  
1939  
1940  
1941  
1942  
1943  
1944  
1945  
1946  
1947  
1948  
1949  
1950  
1951  
1952  
1953  
1954  
1955  
1956  
1957  
1958  
1959  
1960  
1961  
1962  
1963  
1964  
1965  
1966  
1967  
1968  
1969  
1970  
1971  
1972  
1973  
1974  
1975  
1976  
1977  
1978